中國機械工程學刊第四十六卷第四期第 377~385 頁(民國一百一十四年)
Journal of the Chinese Society of Mechanical Engineers, Vol.46, No.4, pp377~385 (2025)

High-Performance Methanation of Carbon Dioxide Using Dual-Functional Materials Loaded with Hydrangea-Like Nickel Catalyst

Yi-Sin Chou* and Yu-Chang Liu**

Keywords：duel function material, titanium nanotube, hydrangea-like Ni catalyst, methanation.

ABSTRACT

A novel dual functional material (DFM) was developed to efficiently convert carbon dioxide into fuel, emphasizing safety, efficiency, and economy. This DFM integrates adsorption and conversion functions, featuring innovative nano-sized nickel (Ni) catalysts and titanium nanotubes (TNT) with a specific surface area of 150.9 m^2/g as supports. The bifunctional material comprises MgO as an alkaline CO_2 adsorbent and Ni as the methanation catalyst. Compared to TNT-based supports, the new DFM improves CO_2 adsorption capacity by over 20 times. Granulated DFMs were fabricated using tablet granulation, offering practical applications for CO_2 methanation in flue gas treatment.

INTRODUCTION

At present, the development of the global economy depend on a large amount of fossil fuels. Due to the continuous growth of energy consumption, the emissions of greenhouse gases such as CO_2 and short-carbon paraffins in the atmosphere have increased substantially, and the greenhouse effect has become an increasingly serious problem (Lee et al., 2021). In view of this, many countries have targets to reduce carbon dioxide emissions. Actively promote compliance with the KyotoProtocol and Paris Agreement norms to establish climate action mechanisms (Falkner, 2016). According to the US Department of Energy (DOE) data, global energy demand will increase by nearly 35 % in 2030 compared with 2005 (Khan et al., 2019). Although the supply of renewable energy sources such as solar and wind power carries on growing, global carbon emissions continue to increase. The international energy agency (NEA) pointed out that global energy demand will still be extremely dependent on fossil fuels in 2030 (Environmental Protection Agency, 2020). The treatment technologies has been proposed and studied about CO_2 capture, conversion, storage, and deep disposal, etc. Among various technologies of carbon capture and utilization (CCU), the most promising technology is CO_2 methanation, where captured CO_2 is converted to methane with higher energy density using hydrogen as a reducing agent, known as called the Sabatier reaction (Otto et al., 2015). The product is directly methane, which can be easily transported through established natural gas pipelines for distribution and utilization (Omodolor et al., 2020). Ru, Rh could be also used as an active metal in dual functional material (DFM) (Erdőhelyi, 2020). Using only 0.1 wt% Rh loading on the Rh-CaO/Al_2O_3 DFM can produce similar amounts of CH_4 as the DFM with 5 wt% Ru. However, the high prices of Rh and Ru hinder their further implementation. Also, the use of Na_2CO_3 and K_2CO_3 adsorbents on Al_2O_3 proved to be a more reliable method to improve DFM performance. The role of Ru in DFM applications was further investigated (Xu et al., 2016; Tada et al., 2014). With Na_2CO_3 or Na_2O-type adsorbent, Ru can exhibit faster hydrogenation rates for excellent methanation kinetics. The research work analyzed the reaction mechanism of combined CO_2 capture and methanation on 5 % Ru, 10% Na_2CO_3 (or 6.1 % Na_2O)/Al_2O_3 DFM using in situ drift (Proaño et al., 2019). In the beginning, Na_2CO_3 originates from Al-O-Na^+ sites and decomposes under reducing atmosphere. Most of the CO_2 in the gas stream is adsorbed by these sites and retained as chelated carbonate complexes. Adsorbed carbonates spill over to nearby Ru sites via formate-type intermediates and hydrogenate to CH_4. Furthermore, using this DFM, with lower amounts of 0.5 % Ru proved useful for combined direct air capture and CO_2 methanation processes (Jeong-Potter et al., 2021). Through this process, CO_2 is captured from ambient air at concentrations as low as 400 ppm. CO_2 can be

Paper Received June, 2022. Revised December, 2024. Accepted December, 2024. Author for Correspondence: Yi-Sin Chou.

* *Associate Researcher, National Atomic Research Institute, Taoyuan, Taiwan 325207, ROC.*

** *Associate Engineer, National Atomic Research Institute, Taoyuan, Taiwan 325207, ROC.*

successfully converted to CH_4 when H_2 flows into the reaction. Although Ni is much cheaper than Ru or Rh, it is not considered useful for DFM in flue gas applications due to its lower reducibility (Arellano-Treviño et al., 2019a). However, the addition of a small amount of noble metals, i.e., 1 wt% Pt and 1 wt% Ru, on the 10 wt% Ni-6.1 wt% Na_2O/Al_2O_3 DFM can enhance the reducibility of Ni by 50 and 70 % at 320 °C, respectively. It is assumed that the PtO_x and RuO_x phases are initially rapidly reduced, and then they in turn split atomic hydrogen and spill over to nearby NiO sites. Due to the synergistic effect between Ni and Ru active metals, the bimetallic 1 wt% Ru-10 wt% Ni-6.1 wt% Na_2O/Al_2O_3 DFM exhibited the highest CO_2 adsorption capacity and CH_4 yield among the studied materials (Arellano-Treviño et al., 2019b). Pt atoms act as additional CO_2 capture sites in the form of Pt-CO species, but they do not contribute to methanation (Proaño et al., 2020). In contrast, Ru sites in RuNi-based DFMs contribute to the methanation process and provide their transport with superior reducibility and catalytic activity utilization of a wide range of natural gas grids (Ashok et al., 2020). Therefore, the need for further study of the novel DFM with high surface areas has become pressing. Anatase and rutile are two mineral forms of titanium dioxide. The reducing ability of anatase titanium dioxide is stronger (Balamurugan et al., 2022). This study attempts to synthesize anatase TiO_2 nanotubes in a relatively low-temperature hydrothermal manner. The development of DFM catalyst is the main key technology. In this study, nickel-based catalysts with low cost and commercialization potential were used, and the preparation technology of nanoscale structure catalysts was applied. Improve the specific surface area of nickel-based catalysts and adsorbents such as MgO and Na_2CO_3. In order to reduce the activation energy on the reaction, and then improve the yield. In addition, an accelerator is added to the nickel-based catalyst to increase the service life of the nickel-based catalyst.

EXPERIMENT

Preparation of TiO_2 nanoparticles and TNT support

A series of TiO_2 nanoparticles were prepared by sol-gel method using acetic acid as the catalytic agent. The sol-gel was prepared from titanium(IV) ethoxide (≥ 99 %, Alfa Aesar) precursors. The solvent used was isopropyl alcohol (ACS reagent, ≥ 99 %, JT Baker®) to give a solvent/precursor molar ratio of 1/1. High purity helium (99.99 %, C.C. GASEOUS CORPORAITON) was flowed through the reactor. This solution was added dropwise to the mixture containing 5.2 moles of acetic acid and 50 moles of DI water (deionized water) cooled at 5 ℃ under helium gas purging and vigorous stirring. In order to increase the stability of sol-gel and control the particle size of TiO_2 nanoparticles, the sol-gel was prepared at 5 ℃ under helium gas purge. Fresh sol-gel solution was transparent without any precipitate. After hydrolysis and condensation, the mixture was heated at 80 ℃ in a water bath for 4 hr. After that, the temperature was gradually decreased to room temperature. The resulting sol-gel was placed into an autoclave to undergo the hydrothermal process, which heated the mixture at 150-250 ℃ for 12 hr. After hydrothermal process, the mixtures were dried to form the TiO_2 bulk at 80 ℃ with a hot water bath, and then the sample was ground as a powder form. To form the anatase phase of TiO_2, the samples were subsequently calcined at 500-900 ℃ for 1 hr. Characteristic of the prepared TiO_2 nanoparticles and calcined sample were determined by nitrogen sorption, XRD and SEM. In order to increase the surface area of support, titanium nanotube (TNT) support was prepared with the above-synthesized TiO_2 nanoparticle powder. We tried to synthesize anatase TiO_2 nanotubes by hydrothermal method at a lower temperature, and the powder was taken out after the reaction was completed. The titanium nanotubes were prepared by pickling at different pH values. The pH values of the solution prepared by hydrogen chloride (ACS reagent, 37 %, JT Baker®) and deionized water was pH 0.8, 1.3, 2.2, 4.0, and 6.5, respectively.

Various of Ni catalyst preparation

Used 1.0 g $Mg(NO_3)_2$ (ACS reagent, ≥ 99 %, Merck®) into a 250 ml beaker filled with 10 ml deionized water (DIW) and stir for 1 hr until completely dissolved. The $Mg(NO_3)_2$ solution was poured into 9.0 g Al_2O_3 (99 %, Alfa Aesar) and stirred for 1 h to make the mixture homogeneous. After drying, it was ground into a powder with a mortar. The operating temperature of furnace was raised to 550 °C at a heating rate of 10 °C/min and calcined for 3 hr. The preparation of 10 % $Mg(NO_3)_2$ on Al_2O_3 carrier (10 % $MgO-Al_2O_3$) was completed. According to the same preparation procedure, 20 and 40 wt% $MgO-Al_2O_3$ magnesium adsorbent impregnated with different concentrations. Used 1.5 g $Ni(NO_3)_2$ (98 %, Alfa Aesar) into a 250 ml beaker filled with 10 ml DIW and stir for 1 hr until completely dissolved. The $Ni(NO_3)_2$ solution was added to 3.5 g 10 % $MgO-Al_2O_3$, and the mixture was continuously stirred for 1 hr, then placed in an oven and dried at 105 °C. After drying 30 %NiO-10 %$MgO-Al_2O_3$, grind it into powder with a mortar. Then moved it into a tubular reduction high-temperature furnace with hydrogen at a heating rate of 10 °C/min to 650 °C. After reducing and calcining for 1 hr, the DFM catalyst of 30 %Ni-10

%MgO-Al_2O_3 was obtained. Duel function material (DFM) with 30 wt% Ni catalyst and 10~40 wt% MgO adsorbent were loaded on TNT powder using the incipient wetness method. The DFM was dried in air at 120 ℃ for 2 hr and calcined in air at 250 ℃ for 2 hr. The nanometer-scale hydrangea-like Ni catalyst and MgO adsorbent coexisting on the surface of mesoporous alumina (MA) support, combined with the addition of a Na_2CO_3-MgO dual adsorbent, is referred to as a dual-functional material (H-AB/MA).

DFM Characteristerization

The gravimetric analysis (TGA) was carried out to implement CO_2 adsorption−desorption measurements under nitrogen purge, adsorption of 10 % CO_2/N_2 at a flow rate of 60 mL/min and desorption with nitrogen purge at 350 °C. About 10 mg DFM sample was loaded in an alumina oxide crucible and heated to set temperature. The N_2 adsorption-desorption measurements was carried out. In this study, the volume flow rate of the tail gas after the reaction was measured by a digital flow meter. The exhaust gas components were analyzed for by a gas chromatography analysis (GC2000, China Chromatography CO., LTD.), and the volume flow rate and molar flow rate of each component were estimated. Calculates CO_2 conversion (X_{CO2}), methane selectivity (S_{CH4}) and methane production rate (Y_{CH4}) to evaluate catalyst performance, and the corresponding equations can be expressed as

$$X_{CO2} = \left[\frac{(\dot{n}_{CO2,in} - \dot{n}_{CO2,out})}{\dot{n}_{CO2,in}} \right] \times 100\% \quad (1)$$

$$S_{CH4} = \left[\frac{\dot{n}_{CH4,out}}{\dot{n}_{CO2,in} - \dot{n}_{CO2,out}} \right] \times 100\% \quad (2)$$

$$Y_{CH4} = \left[\frac{\dot{n}_{CH4,out}}{\dot{n}_{CO2,in}} \right] \times 100\% \quad (3)$$

where $\dot{n}_{CO2,in}$ is input molar flow rate of CO_2, $\dot{n}_{CO2,out}$ is output molar flow rate of CO_2 , and $\dot{n}_{CH4,out}$ is output molar flow rate of CH_4. A U-shaped reactor was filled with 0.1 g of DFM catalyst immobilized. The front and rear ends are filled with quartz wool to fix the DFM catalyst to avoid spraying, and the reaction volume in the reactor was fine-tuned and placed in a high-temperature furnace. First, a fixed amount of CO_2 gas was introduced for adsorption for 1 hr, and then a quantitative amount of H_2 was introduced for reduction and conversion reaction. When the catalyst was applied with energy, the incoming CO_2 was decomposed by reducing the activation energy of the catalyst. Through the reactive sites on the surface, it combined with hydrogen protons to carry out catalytic reduction reaction to generate CH_4, CO, etc. Samples were taken every 1 hr, and the gas reacted through this reactor was analyzed by GC. Through calibration curve calculation, the generated gas content could be known.

Results and Discussions

The TiO_2 powder is calcined at different temperatures for one hr under normal conditions. The XRD diffraction pattern is shown in Fig. 1. It is observed that the sintering temperature is lower than 800 °C, the crystal structure is dominated by anatase structure, and no rutile crystal phase is produced. The possible factor is that the calcination time is insufficient, and there is not enough calcination time to produce a change in the crystal form. When the sintering temperature is above 800 ℃, the rutile phase appears at $2\theta \fallingdotseq$27.5, 36.2, 39.2, 41.3, 44, 54.1, 57.7, and 64. In order to reduce the temperature required to synthesize anatase TiO_2, the desired TiO_2 nanomaterials were synthesized by hydrothermal method under different pH conditions in an autoclave. In order to increase the specific surface area of the support, this research further developed titanium dioxide nanotubes (TNT), which can be expected to increase the amount of reactive bases for CO_2 reactions. We tried to synthesize anatase TiO_2 nanotubes by hydrothermal method at a lower temperature, and the powder was taken out after the reaction was completed. The titanium nanotubes were prepared by pickling at different pH values. The pH values of the HCl solutions were pH 0.8, 1.3, 2.2, 4.0, and 6.5, respectively. When the initial anatase lattice-like TiO_2 precursor reacts in NaOH, its Ti-O bond will be broken slowly. A sheet-like or layered structure is gradually formed, which is an intermediate product of the nanotube-forming reaction. After the pickling process, the sheet-like structure will gradually form a tube-like structure in a curling manner. Therefore, the pickling procedure becomes particularly important in the process of forming titanium tubes. The XRD crystal phase analysis diagram of the support prepared under different acid washing conditions are illustrated in Fig. 2. The crystal phase of the reaction precursor is obvious anatase TiO_2. During pickling process at pH 6.5, the diffraction peaks of $Na_2Ti_2O_5 \cdot 5\ H_2O$ and $Na_2Ti_3O_7$ can be seen at about 2θ=28.2°. During pickling process, the supply of H^+ is not sufficient to replace Na^+. Therefore, the resulting support powder is a titanate structure, not titanium dioxide. When the pH value during pickling process is reduced to 4.0 and 2.2, there is only a very weak diffraction peak of titanate at 2θ=28.2° compared with 2θ=25.2°. It can be seen that the Na^+ ions in this titanate are more affected by H^+ replaced. When the pH value of the pickling process is further reduced to 1.3 and 0.8, it is obvious that the diffraction peak of titanate is no

longer visible at 2θ=28.2°, and the intensity of the diffraction peak at 2θ=25.2° becomes much stronger. This is the (1,0,1) crystal plane of TiO_2 anatase, and the various crystal planes of the anatase crystal phase can also be seen from other angles. Therefore, the pH control of the pickling procedure during the synthesis process will seriously affect the degree of H^+ ions replacing Na^+ ions, which will affect the structure and crystal phase of the nanotube products.

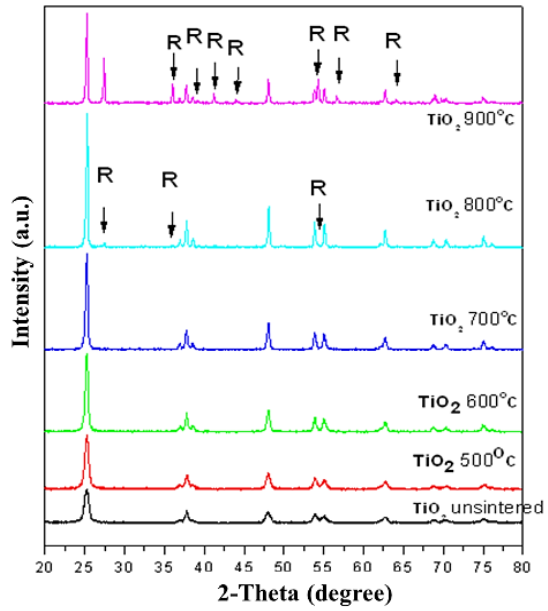

Fig. 1. XRD diffraction of rutile TiO_2 nanopowder prepared calcined at various temperature.

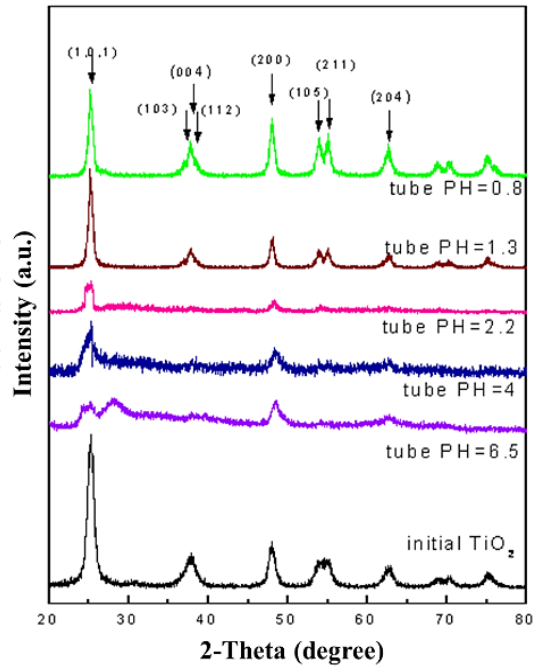

Fig. 2. XRD diffraction of anatase titanium tubes prepared by acid washing with different pH values.

According to EDX characteristic analysis as shown in Fig. 3, the element ratio of titanium and oxygen is 1:2, which can prove that the composition of the synthesized compound is indeed titanium dioxide, and no other complex is formed. The slurry at different temperatures was freeze-dried into powder, and the surface morphology of the powder material was observed by SEM. The particle size distribution of the titanium dioxide powders prepared at the various hydrothermal temperature. The particle size distribution and particle size of TiO_2 increase with the increase of hydrothermal temperature. The comparison on the particle size and shape of the titanium dioxide particles is carried out using different hydrothermal temperatures as shown in Fig. 4. When the titanium dioxide slurry is prepared at a hydrothermal temperature of 150 °C, the particles of TiO_2 are small, and titanium dioxide particles are relatively densely arranged. In addition, the pores between the particles are relatively small and less porous as shown in Fig. 4 (A). Fig. 4 (B) shows the loose structure of titanium dioxide particles due to the increase of the particle size of TiO_2, when the hydrothermal temperature is 190 °C. As illustrated in Fig. 4 (C) and (D), titanium dioxide particles grow longer. There is obvious block formation and local aggregation of particles leads to the appearance of large pores, when the hydrothermal temperature reaches 220 and 250 °C. The results are similar to using titanium isopropoxide as a raw material (Döscher, H. et al., 2016). When the hydrothermal temperature is lower, the particle size of TiO_2 becomes smaller, as shown in Table 1. Using this low-temperature hydrothermal synthesis condition, the specific surface area of TiO_2 particles is increased, and the pore size between relative particles becomes smaller. Therefore, proper temperature regulation can control the titanium dioxide particles to reach the required size. The TiO_2 powder synthesized at the hydrothermal process temperature of 200 ℃ was taken as the follow-up research object and the modification of co-catalyst. The SEM surface morphology of the TiO_2 nanopowder obtained by the sol-gel method. The particle distribution is very uniform, and the size of a single particle is about 20 nm as shown in Fig. 5. The interior is rich in pores and the particle size of the powder is small, and the particles on the crystal surface are relatively uniform and dispersive. The anatase TiO_2 is used as a reaction precursor for the preparation of nano-titanium tubes.

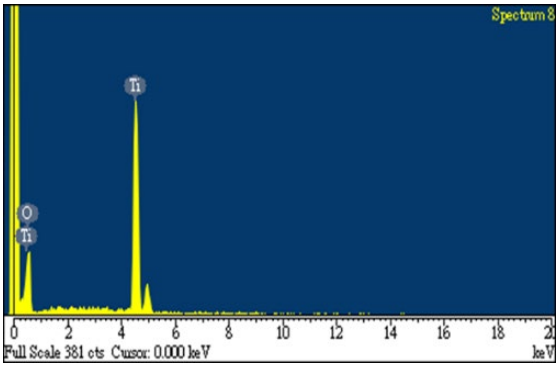

Fig. 3. EDX pattern of TiO_2 powder synthesized at the hydrothermal process temperature of 200 ℃.

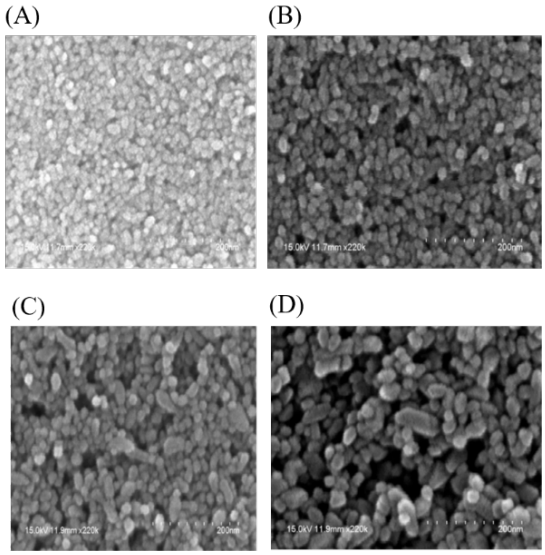

Fig. 4. The surface morphology of nano-TiO_2 powders prepared with hydrothermal method at (A)150, (B)190, (C) 220 and (D) 250℃.

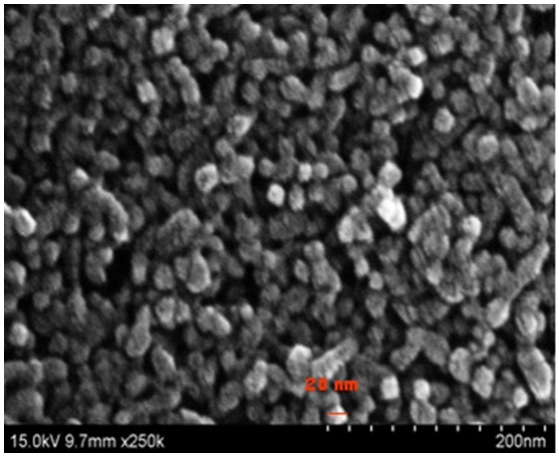

Fig. 5. The surface morphology of nano-TiO_2 powders prepared with sol-gel method at 200 ℃.

Table 1. The average diameter of TiO_2 nanopowder prepared with hydrothermal method at various temperatures.

Temperatures (℃)	Average diameter (nm)
150	10~20
170	15~25
190	20~30
200	20~30
210	20~40
220	30~45
230	30~45
240	35~50
250	40~65

The specific surface area of the precursor TiO_2 is only 150.9 m^2/g. Titanium tubes were obtained by the sol-gel method. Table 2 shows the specific surface area of titanium tubes prepared by acid washing procedures with pH 0.8, 1.3, 2.2 and 6.5, respectively. at Due to the insufficient degree of pickling and only a small amount of Na^+ ions replaced by H^+ at pH 6.5, the sheet-like titanate is only slightly partially curled into a tubular shape. Therefore, the specific surface area is only slightly increased to 161.6 m^2/g. For the titanium tube with pickling at pH 2.2, the proportion of Na^+ ions inside is greatly reduced due to the increase in this degree of pickling condition. The ratio of sheet-shaped titanium oxide or titanium oxide to be rolled to form a titanium tube is increased, and the specific surface area is 294.9 m^2/g. When acid pickling at pH 1.3, the specific surface area of the support reaches a maximum value of 381.2 m^2/g. At this time, its structure is fluffy and the porosity should be the largest. However, when the pickling condition is lowered to pH 0.8, the structure of the titanium tube is gradually destroyed by the acidity and begins to be defective. Therefore, the specific surface area decreases to 335.1 m^2/g, and the porosity also becomes to decrease. The specific surface area of this catalyst-reduced support configuration is much higher than that of the general reduced nickel support (~ 1 m^2/g). Whether it is a powder or a titanium tube, the synthesized support is about 3 to 7.4 times that of P25 TiO_2 (25% anatase, 75% rutile, ACS Material, LLC) with a specific surface area of 52.1 m^2/g. Besides increasing the specific surface area, the smaller particles of the support also change the quantum efficiency of the electron-hole pairs generated by absorbing energy. Small particles not only increase the redox potential of electrons and holes, but also delay the process of releasing energy from the excited state. So that more electrons can be transferred to the decomposed substance on the adsorption surface, thus increasing its catalytic activity.

Table 2. Characteristics of different titanium nanomaterials.

TiO_2 materials	Surface area (m^2/g)	Pore volume (cm^3/g)	Pore size (nm)
Nanotube synthesized at pH=6.5	161.6	0.17	4.28
Nanotube synthesized at pH=2.2	294.9	0.24	3.28
Nanotube synthesized at pH=1.3	381.2	0.36	3.76
Nanotube synthesized at pH=0.8	335.1	0.29	3.48
TiO_2 (P25, Merck®)	52.1	0.13	10.12
TiO_2 nanopowder	150.9	0.17	4.37

The SEM images of the TiO_2 nano-titanium tube produced by the TiO_2 treated with alkali solution and pickling at pH 1.3, which magnifies to 10, 50, 100 and 300 K, are shown in Fig. 6. Fig. 6 (A) is a macroscopic view of SEM at low magnification. It can be seen that the internal structure of the catalyst is very uniformly distributed, and there is no condition that the reaction is incomplete and still remains as a particle. Fig. 6 (B) shows that the catalyst is in the shape of a tube. Moreover, it is arranged radially in bundles, not in a messy staggered state. Fig. 6 (C) shows that the tube length of the synthesized TiO_2 nano-titanium tube is at least longer than 1 μm. Fig. 6 (D) is observed that the outer diameter of the TiO_2 nano-titanium tube is 10 nm. The preparation of titanium nanotubes from TiO_2 powder will greatly increase its specific surface area and effectively improve the transmission efficiency of electrons.

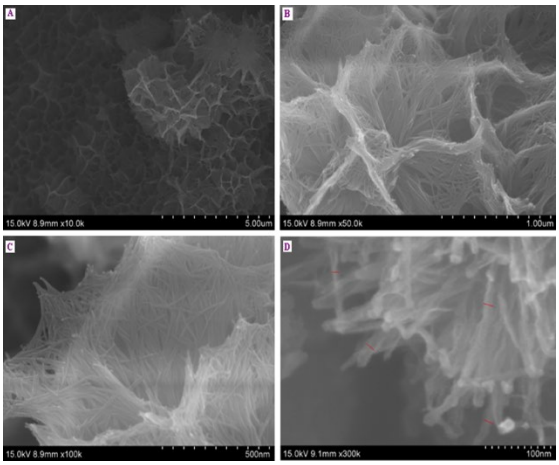

Fig. 6. SEM images of nanotube synthesized at pH 1.3 with magnification of (A) ×10 K, (B) ×50 K, (C) ×100 K and (D) ×300 K

CO_2 has a double bond, C-C connection is very strong, coupled with the connection of oxygen, so the stability is very high. Generally, it is necessary to input very high external energy to break the strong bond of its connecting bond. Therefore, additional energy is required to break its bonds. The SEM photos of the self-developed Ni (hydrangea-like)-MgO/TNT bifunctional catalyst, 30 % Ni-40 % MgO/TNT, are shown in Fig. 7. A schematic diagram of nickel catalysts loaded on TNT-based duel function material for carbon dioxide methanation are shown in Fig. 8. Titanium tube (TNT) support was prepared from the TiO_2 metal oxide nanopowder with the aforementioned excellent characteristics, MgO adsorbent and reduced metal nickel (Ni) were added to the TNT support. It can effectively increase the adsorption and electron transfer efficiency of CO_2, and form methane fuel by thermal catalytic hydrogenation, as shown in Table 3. Using different support (TNT and Al_2O_3), it can effectively adsorb CO_2 and increase the reaction concentration of CO_2 around the DFM catalyst, thereby increasing the conversion rate. The preliminary test results show that the methane conversion rate can be 90 %, and the carbon dioxide adsorption capacity can reach 0.71 mmol/g DFM. Compared with TNT support, 30 %Ni-10 %MgO/Al_2O_3 and 30 %Ni-40 %MgO/Al_2O_3, the average carbon dioxide adsorption capacity is only 0.031, 0.349 and 0.379 mmol/gDFM, respectively. Fig. 9 shows the comparison of thermal conversion methanation of DFM catalyst at 350 °C with the addition of MgO adsorbent on TNT support. The 30 %Ni-10 %MgO/TNT, 30 %Ni-20 %MgO/TNT and 30 %Ni-40 %MgO/TNT catalyst start to react after 1 hr of adsorption, and the average CO_2 conversion (X_{CO2}) are all coming to 87 %. The CH_4 selectivity of 30 %Ni-20 %MgO/TNT and 30 %Ni-40 %MgO/TNT catalyst are 100 % on average, which is better than 95 % of 30 %Ni-10 %MgO/TNT. The results show that adding MgO adsorbent will enhance the selectivity. The CH_4 yields of 30 %Ni-10 %MgO/TNT is the highest at 45 %. The conversion of CO_2 into CH_4 is directly related to Ni metal.

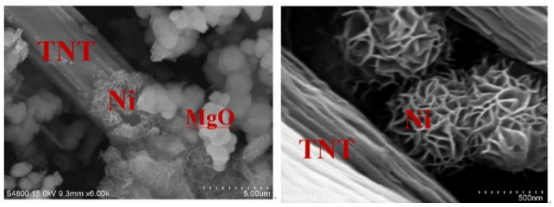

Fig. 7. SEM image of Ni (hydrangea)-MgO/TNT bifunctional catalyst (30 % Ni-40 % MgO/TNT).

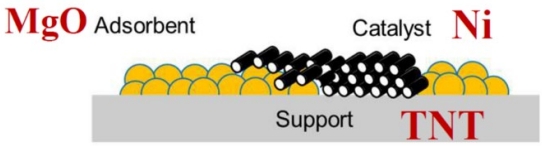

Fig. 8. A schematic diagram of nickel catalysts loaded on TNT-based duel function material for carbon dioxide methanation

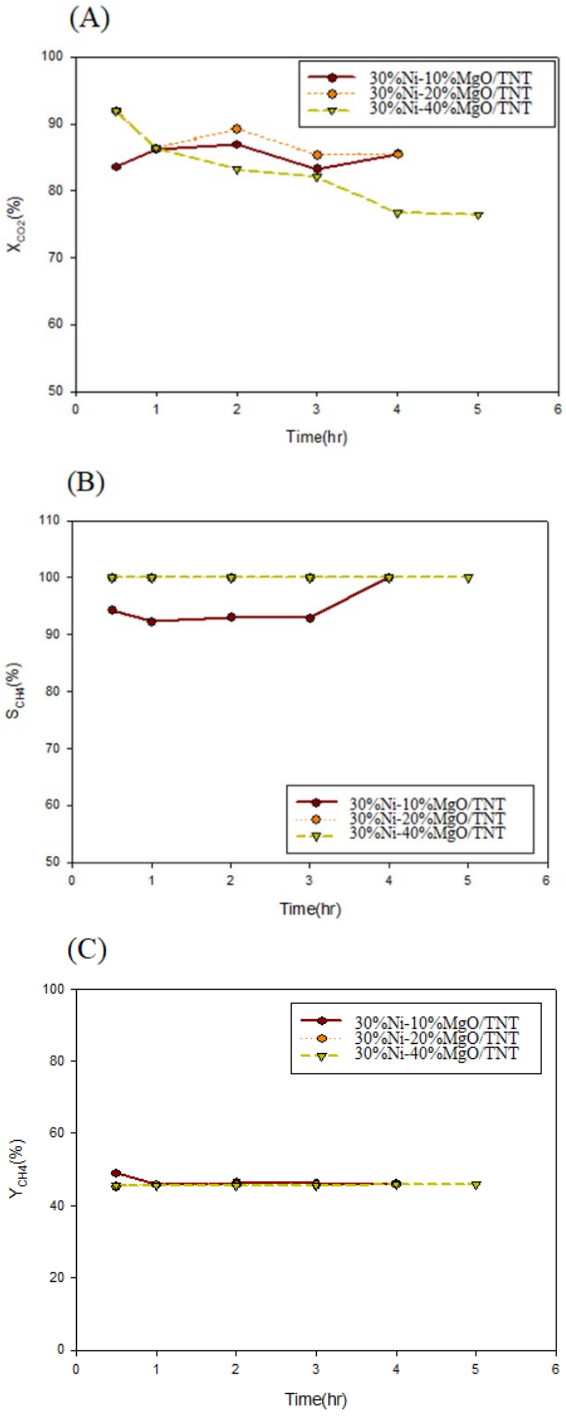

Fig. 9. Plot of (A) CO_2 conversion (X_{CO2}), (B) methane selectivity (S_{CH4}) and (C) methane production rate (Y_{CH4}) for evaluating catalyst performance of 30 %Ni-10 %MgO/TNT, 30 %Ni-20 %MgO/TNT and 30 %Ni-40 %MgO/TNT.

Table 3. Methanation performance of TNT support and nickel catalysts with different composition ratios.

DFM catalyst	CO_2 capture capacity (mmol CO_2/gDFM)
TNT	0.031
30 %Ni-10 %MgO/TNT	0.533
30 %Ni-20 %MgO/TNT	0.589
30 %Ni-40 %MgO/TNT	0.711
30 %Ni-10 %MgO/Al_2O_3	0.349
30 %Ni-40 %MgO/Al_2O_3	0.379

In this study, a dual-adsorbent DFM (H-AB/MA) prepared using mesoporous alumina support was developed. Due to its higher specific surface area and CO_2 adsorption capacity, the DFM achieved a CO_2 conversion rate of up to 84.5 % in an experimental thermocatalytic reactor, with a lower CO yield. Its methane selectivity reached 90 %, suggesting that the reaction pathway likely follows direct CO_2 methanation. In comparison, the DFM based on commercial alumina support (H-AB/GA) exhibited a CO_2 conversion rate and methane selectivity of 81.8 and 85.9%, respectively, indicating that the dual-adsorbent DFM effectively enhances methanation performance. Using H-AB/MA as the DFM, multiple CO_2 adsorption-reduction methanation cycle tests were conducted at 350 °C (as shown in Fig. 10). The results demonstrated that the DFM maintained stability over 112 hrs of reaction, with CO_2 conversion rates and methane selectivity consistently remaining at 83 and 89 %, respectively, without any signs of activity degradation.

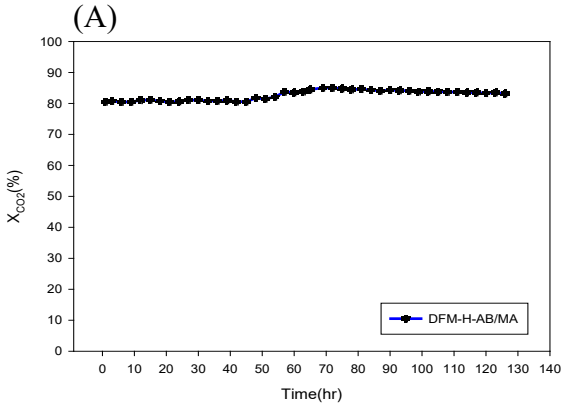

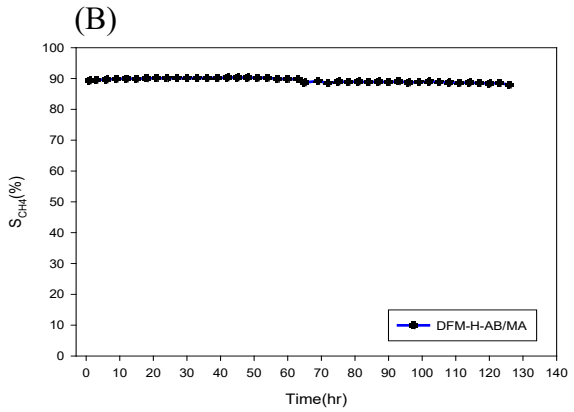

Fig. 10. CO_2 adsorption-methanation cycle test of H-AB/MA (A) CO_2 conversion rate and (B) methane selectivity.

To facilitate the development of the DFM technology in this study and its future practical application, granulated DFM was prepared using tablet granulation technology and loaded into a pilot-scale thermocatalytic conversion system. Tests were conducted at the radioactive liquid waste treatment facility of this institute, using actual flue gas as the feedstock. The radioactive liquid waste treatment facility primarily handles radioactive inorganic liquid waste and is equipped with steam-generating boilers, evaporators, adsorption towers, ion exchange towers, and high efficiency particulate air filter (HEPA). The composition of the flue gas from the facility's boiler includes 13.8 % CO_2, 6.7 % O_2, 40.2 ppm NOx, and 1.2 ppm SOx. Using this as the feedstock, the study aimed to observe the CO_2 adsorption capacity and methane conversion selectivity of the DFM in actual flue gas conditions. CO_2 adsorption and conversion reactions were carried out using the pilot-scale thermocatalytic conversion system. The pilot-scale thermocatalytic reactor test was conducted in three stages: heating, adsorption, and conversion. Initially, nitrogen gas was used as the heating gas, with a flow rate of 1–2 L/min, and the temperature was raised to 350 °C. The subsequent adsorption process involved using an induced draft fan to introduce boiler flue gas into the reactor at a flow rate of 1 L/min. The adsorption test lasted for 1 hr, with the temperature maintained at 350 °C. After adsorption, a nitrogen purge was conducted for 1 minute to eliminate residual oxygen in the pipelines. Finally, hydrogen gas was introduced for the conversion process for 1 hr, with a volumetric flow rate of 60 L/h. The CO_2 conversion rate, methane selectivity, and methane yield achieved were 80.1, 88.0, and 70.5 %, respectively, slightly lower than the results obtained in laboratory-scale thermocatalytic reactors under 100% CO_2 conditions.

CONCLUSIONS

In this study, the nano-hydrangea-like nickel catalysts configuration was developed by a hydrothermal method. It has a significant effect on the improvement of the specific surface area, and also has a significant improvement in relation to the reaction site and activity. The TiO_2 nano-scale powder with nano-scale mesoporous pores is prepared by the sol-gel method and the titanium tube is prepared by the alkali-dissolved hydrothermal method. This TiO_2 nanopowder has a very high specific surface area (381.2 m^2/g), which is larger than that of the general commercial TiO_2 P25 (52.1 m^2/g). Titanium tube (TNT) support was prepared from the TiO_2 metal oxide nanopowder with the above-mentioned excellent properties, and MgO adsorbent was added to reduce metal nickel (Ni) and supported on the TNT support, which can effectively increase the CO_2 adsorption and electron transfer efficiency. The results show that the proportion of MgO impregnation increases, and the carbon dioxide adsorption capacity does not increase proportionally. Using thermal catalytic hydrogenation to form methane fuel, the methane conversion rate can reach more than 90%, and the carbon dioxide adsorption capacity can reach 0.71 mmol/g DFM. Analyze the characteristic of catalyst-TNT for CO_2 conversion reaction during 5 hr to calculate conversion (X_{CO2}), methane selectivity (S_{CH4}) and methane production rate (Y_{CH4}). The granulated dual-functional material (DFM) developed in this study demonstrated significant potential for CO_2 adsorption and methanation in industrial flue gas conditions. Pilot-scale tests using radioactive flue gas achieved high CO_2 conversion rates (80.1 %) and methane selectivity (88.0 %), confirming the effectiveness of the DFM. The material maintained stability during extended operation, with consistent CO_2 conversion and methane selectivity over 112 hrs, showing no degradation in performance. Despite slightly lower yields compared to laboratory-scale reactors, the results highlight the feasibility of DFM technology for practical applications. Future work should focus on cost optimization and long-term industrial scalability. The innovative dual-function catalyst for CO_2 converting CH_4 can is expected to be established a closed carbon cycle in the future.

ACKNOWLEDGEMENT

The authors express their gratitude to the National Atomic Research Institute for providing the necessary funding, equipment, and consumables for the experiments.

REFERENCES

Arellano-Treviño, M. A. He, Z., Libby, M. C. and Farrauto, R.J., "Catalysts and adsorbents for CO_2 capture and conversion with dual function materials : Limitations of Ni-containing DFMs for flue gas applications", J. CO_2 Util., 31, 143–151(2019a).

Arellano-Treviño, M. A., Kanani, N., Jeong-Potter, C. W. and Farrauto, R. J., "Bimetallic catalysts for CO_2 capture and hydrogenation at simulated flue gas conditions", Chem. Eng. J., 375, 121953 (2019b).

Ashok, J., Pati, S., Hongmanorom, P., Tianxi, Z., Junmei, C. and Kawi, S., "A review of recent catalyst advances in CO_2 methanation processes", Catal. Today, Vol. 356, pp. 471–489 (2020).

Balamurugan, M., Silambarasan, M., Saravanan, S. and Soga, T., "Synthesis of anatase and rutile mixed phase titanium dioxide nanoparticles using simple solution combustion method", Physica B, Vol. 638, pp. 413843 (2022).

Döscher, H., Young, J. L., Geisz, J. F., Turner,,J. A. and Deutsch, T. G., "Solar-to-hydrogen efficiency: shining light on photoelectrochemical device performance", Energy Environ. Sci., Vol. 9, pp. 74 (2016).

Environmental Protection Agency, Greenhouse Gas Emission Statistics (2020).

Erdőhelyi, A., "Hydrogenation of carbon dioxide on supported Rh catalysts", Catalysts, Vol. 10, Issues 2, pp.155 (2020).

Falkner, R., "The Paris Agreement and the new logic of international climate politics, International Affairs", Vol. 92, Issues 5, pp. 1107-1125 (2016).

Jeong-Potter, C.W. and Farrauto, R. J., "Feasibility study of combining direct air capture of CO_2 and methanation at isothermal conditions with dual function materials", Appl. Catal. B Environ., Vol.282, pp. 119416 (2021).

Khan, A. A. and Tahir, M., "Recent advancements in engineering approach towards design of photo-reactors for selective photocatalytic CO_2 reduction to renewable fuels", Journal of CO_2 Utilization, Vol. 29, pp. 205-239 (2019).

Lee, W. J., Li, C., Schiebahn, S., Prajitno, H., Yoo, J., Patel, J., Yang, Y. and Lim, S., "Recent trend in thermal catalytic low temperature CO_2 methanation: a critical review", Catalysis Today, Vol. 368, Issues 15, pp. 2-19 (2021).

Omodolor, I. S., Otor, H. O., Andonegui, J. A., Allen, B. J. and Alba-Rubio, A. C., "Dual-function materials for CO_2 capture and conversion: a review", Ind. Eng. Chem. Res., Vol. 59, pp. 17612-17631 (2020).

Otto, A., Grube, T., Schiebahn, S. and Stolten, D., "Closing the loop: captured CO_2 as a feedstock in the chemical industry", Energy & Environmental Science, Vol. 8, pp. 3283-3297 (2015).

Proaño, L., Arellano-Treviño, M. A., Farrauto, R.J, Figueredo, M., Jeong Potter, C. and Cobo, M., "Mechanistic assessment of dual function materials, composed of Ru-Ni, Na_2O/Al_2O_3 and Pt-Ni, Na_2O/Al_2O_3, for CO_2 capture and methanation by in-situ DRIFTS", Appl. Surf. Sci., Vol. 533, pp. 147469 (2020).

Proaño, L., Tello, E., Arellano-Treviño, M. A., Wang, S., Farrauto, R.J. and Cobo, M., "In-situ DRIFTS study of two-step CO_2 capture and catalytic methanation over Ru,"Na_2O"/Al_2O_3 dual functional material", Appl.Surf. Sci., Vol. 479, pp. 25–30 (2019).

Tada, S., Ochieng, O. J., Kikuchi, R., Haneda, T. and Kameyama, H., "Promotion of CO_2 methanation activity and CH_4 selectivity at low temperatures over $Ru/CeO_2/Al_2O_3$ catalysts", International Journal of Hydrogen Energy, Vol. 39, pp.10090-10100 (2014).

Xu, J., Lin, Q., Su, X., Duan, H., Geng, H. and Huang, Y., "CO_2 methanation over TiO_2-Al_2O_3 binary oxides supported Ru catalysts", Chinese Journal of chemical Engineering, Vol. 24, Issues 1, pp. 140–145 (2016).